MASTER OF SCIENCE THESIS

The effect of impurity of CO_2 stream on enhanced gas dissolution

Author:
Gerrit van Loenen

Supervisor:
Dr. Denis V VOSKOV

to obtain the degree of Master of Science
at the Delft University of Technology,
to be defended publicly on Thursday November 30, 2017 at 13:00.

Student number: 1371703
Specialisation: Petroleum Engineering
Thesis committee:
Dr. D. V. Voskov, TU Delft, supervisor
Prof. Dr. Ir. J. D. Jansen, TU Delft
Prof. Dr. J. Bruining, TU Delft
Dr. A. Barnhoorn, TU Delft

TU Delft

Abstract

One of the methods of reducing the amount of CO_2 in the air is CO_2 sequestration by dissolving the gas underground in an aquifer. In practice, there will be impurity gases in the injected CO_2 stream or in the aquifer, which influence the dissolution rate of the CO_2 stream. This research aims at finding a method to evaluate and calculate this influence. We focused on H_2S and CH_4. We found that given the specific circumstances underground and with added impurity gases, it is advisable to use an Equation of State, for which we chose Peng-Robinson. For the first simulation with a large aquifer model, we were able to see the difference between a stream of pure CO_2 and mixtures of CO_2 with H_2S and CH_4 respectively. We observed that the gas stream with CH_4 moved considerably faster along the aquifer than the streams of pure CO_2 or CO_2 mixed with H_2S. On the other hand, we found that the dissolution rate was higher when H_2S was present in the mixture. In the dissolution process, we see a large influence of instabilities on the dissolution rate as a result of density differences in the aquifer. However, the resolution of the large aquifer model did not allow to evaluate this influence sufficiently. In two consequent steps, we adapted our simulation model. First, we used a small scale model using only a fraction of the large aquifer model, thus considerably reducing the calculation time. Next, we increase the resolution of the small scale model. This higher resolution gave considerably more accurate results, reflecting the differences between the three cases and the influence of the instabilities in the aquifer. We concluded that the simulation based on the small scale and high resolution model yields accurate and reliable results. However, the calculated outcomes have to be corrected for the difference in boundary conditions between the large and small scale models.

Contents

1 Introduction

1.1. Structure of the report

In this report, we will study the influence of impurity of a CO_2 stream on the process of gas dissolution in an aquifer. In chapter 1, we will briefly sketch the background for CO_2 storage and related research and define the objectives and the different steps that will be taken in the research. Subsequently, we will describe these steps in chapters 2 to 4. Chapter 5 will conclude this paper with a short summary and recommendations.

1.2. Background

In the last decades, the world has become increasingly interested in the effect of greenhouse gases such as carbon-dioxide, CO_2, which is released into the air in large amounts by burning fossil fuels - oil, gas or coal [15]. Though the exact scale of the effect of these man-made greenhouse gases on the world climate is yet unknown, it is nevertheless useful to search for methods which could reduce the CO_2 emission [3]. Application of alternative sources of energy, such as wind or solar power for example, do not lead to substantial amounts of greenhouse gases in the air. However, their contribution to the energy landscape is still marginal in comparison to fossil fuels.

Apart from reducing the CO_2 emission, another possibility to reduce the amount of CO_2 in the air is to store the gas in the subsurface. Storing CO_2 can be performed in three different ways [9]: terrestrial sequestration [14], mineral sequestration [1] and geologic sequestration [4]. Terrestrial sequestration involves storing the CO_2 in vegetation by expanded forestation. Geologic sequestration of CO_2 refers to a method of trapping the CO_2 underground. The trick is to store the gas in - for example - depleted oil and gas reservoirs where it gets trapped by the conditions that previously kept the oil and gas trapped. Lastly, CO_2 can be stored by having it react with certain minerals to create carbonate salts, which is called mineral sequestration. This is the most permanent but also the slowest mechanism of trapping CO_2; it can take several millions of years to trap CO_2 completely by mineral sequestration. Of these different methods of storing CO_2, we will focus on storing CO_2 underground by injecting it in aquifers.

Aquifers are layers of permeable rock bearing (saline) water. CO_2 can be injected into these aquifers and trapped there by different mechanisms: geologic, residual, dissolution and mineral trapping [5]. The residual and geologic trapping are the fastest mechanisms to store CO_2. However, the amount of CO_2 that can be stored this way is limited. Residual trapping means that a part of the gas that flows through an aquifer will leave small bubbles of gas behind in the pores filled mostly with water, which can result in a residual gas saturation of 20% [11]. Dissolution trapping is storing the CO_2 by dissolving it in the aquifer, and this process is what we are going to look at. Once dissolved, the gas can be further stored through mineralization.

The total amount of CO_2, that can be sequestered in an aquifer, is primarily a function of the rate at which CO_2 is immobilized by the different trapping mechanisms, as well as the geologic 'quality' of the aquifer based on its overall size, permeability characteristics, the relative impermeability of the caprock, and the absence of major geologic faults and fractures [13]. The longer the time that the injected CO_2 remains in contact with

the caprock (due to its buoyant supercritical state with respect to the resident fluid), the greater is the risk of the CO_2 leakage. Vertical and up-dip migration of large-scale CO_2 plumes over long periods of time also adds to the risk of leakage. Moreover, changes in the pressure field due to injection of large amounts of CO_2 may lead to the activation or creation of fractures and faults that provide CO_2 leakage pathways beyond the target formation. It follows that a fundamental objective of CO_2 sequestration operations is to maximize the overall amount of injected CO_2 while minimizing the risk of leakage.

In order to plan, execute, and monitor field-scale CO_2 sequestration operations, accurate modeling of the physical and chemical processes that govern solubility, capillary and mineral trapping in subsurface geologic formations is necessary [7, 12]. For that purpose, the complex dynamics associated with the various trapping mechanisms and their interactions must be analyzed in details and modeled accurately. That is, the governing equations must be formulated rigorously, and the length and time scales that govern the physical and chemical processes associated with subsurface CO_2 sequestration must be resolved adequately. Then, using a detailed characterization model for the specific storage target, high-resolution numerical simulation can be used to make quantitative predictions of the complex dynamics associated with field-scale CO_2 sequestration operations. The simulation capability must be able to cover the (relatively short) injection and the (much longer) post-injection periods.

The process of dissolution is influenced by many factors such as pressure, temperature, gravitational forces and other gases present in the injected stream or already present in the reservoir. Some common extra gases (subsequently referred to as impurities) are nitrogen (N_2), hydrogen sulfide (H_2S) and methane (CH_4). This research project aims at modeling the dissolution trapping of a CO_2 stream with impurities. We will use a set of 2D models, filled with a large amount of either pure CO_2, or CO_2 accompanied by other gases such as CH_4 or H_2S.

The gases will slowly dissolve unevenly (due to small heterogeneities in the ground) into the aquifer causing density differences in the aquifer. Because of gravity, these irregular density differences of the water will cause unstable convection of the denser water downwards. The interplay between diffusion and convection can enhance the dissolution in several folds [6]. The enhanced dissolution mechanism can provide a significant volume for trapping of CO_2 in the subsurface within a reasonable timescale of the process [10]. An accurate prediction of this enhanced dissolution process is the main target of this research project.

For the simulation of the CO_2 sequestration process, the Stanford's in-house Automatic Differentiation General Purpose Research Simulator (ADGPRS) is used, which has capability to perform simulation of multiphase multi-component reactive flow and transport [20, 22, 23]. This framework was already used in the convergence study of CO_2 sequestration processes with enhanced convective dissolution [6] and chemical reactions [21], which makes it a logical choice for the current research.

1.3. Objectives

The objective of this research is to determine the impact of impurities in a CO_2 stream on the process of enhanced gas dissolution. For clarity, 'enhanced CO_2 dissolution' will be interpreted in this paper as the entire process of CO_2 spreading through the reservoir: both CO_2 dissolving in water at the interface with the CO_2 plume and the buoyancy driven convection of water saturated with dissolved CO_2.

In this research, we will perform the analysis of numerical solutions obtained in ADGPRS. For predictive simulations, it is important to use an accurate Equation of State (EoS). In chapter 2, we will explain the background of various equations of state and validate our choice against the results presented in [2]. We will conclude on the most appropriate choice of EoS to be used in the further investigation related to impurities in CO_2 stream.

Additionally, in chapter 2, we will demonstrate the effects of CO_2 instabilities (which will be referred to as fingers) to the macroscopic dissolution in the brine (salted water). These instabilities are a result of the interplay between gravity and diffusion, where gas-saturated water is slightly heavier than the surrounding unsaturated water, which forces it to flow downward. This flow, or convective fingering, plays an important role in CO_2 dissolution trapping and is the main focus of this research.

In the following chapters, the effect of impurities, present in the CO_2 stream, on the enhanced dissolution of gas will be determined and quantified. Two common impurities are considered for their different properties and solubilities in water: (a) methane (CH_4), which is less soluble than CO_2, and (b) H_2S, which is more soluble than CO_2. We intend to determine the respective dissolution rates of CO_2 stream with these gases added.

In chapter 3, a slightly tilted 5 km wide and 50 m high aquifer is chosen as a synthetic model which represents a typical aquifer, see the example in Fig. 1.1. The CO2 gas is injected into the lower side and initially travels up and then sideways along the top of the reservoir in the up-dip (upward) direction. Part of this gas will dissolve in the aquifer and move down due to gravity, forming unstable fingers and spreading through the reservoir. The objective here is to follow the total amount of gas dissolving in brine. A characteristic control volume is defined which consists of a 400 m wide vertical slice of the reservoir, in order to look closely at the vertical movement of dissolved gas. Using this model, we will study the effect of impurities on the CO_2 dissolution during this process.

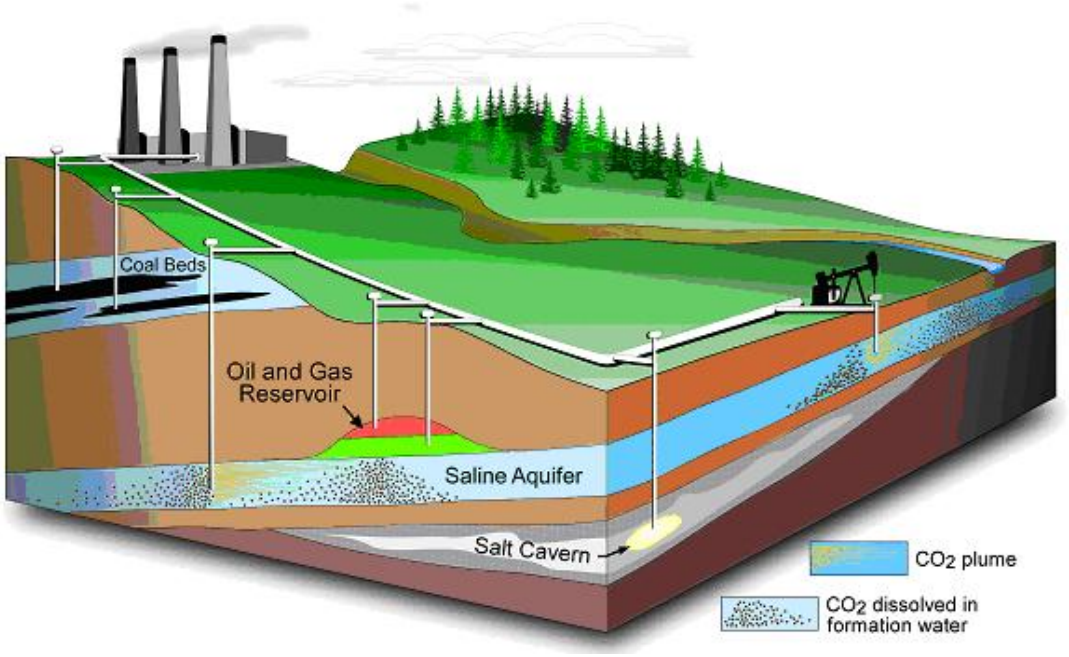

Figure 1.1: Example CO2 injected in aquifer: CO_2 sequestration (Source: Alberta Geological Survey)

The simulations of the large scale model, studied in chapter 3, took over 11 hours to complete, yet the resolution of this model is rather coarse to represent the enhanced dissolution process accurately enough. In chapter 4, we will investigate whether we can improve the computation time by extracting an enhanced dissolution rate using small scale simulation models. In section 4.1, we will show the results of a simulation using a small scale model of 400 m wide and 50 m high, with the same gridblock size as in in chapter 3. Subsequently, in section 4.2, we will increase the resolution of this model to check the convergence of the numerical solution. In section 4.3, we address the question whether the results predicted by this small-scale model will match the dissolution rate of the large-scale model, studied in chapter 3. The appropriate correction ratio will be proposed as well for this small scale dissolution rate.

2

Regimes of CO_2 sequestration

In this chapter, two different regimes of CO_2 sequestration will be modeled. The first regime corresponds to the injection stage, when CO_2 is mostly immobilized by residual trapping. However, as we are going to demonstrate, the Equation of State (EoS) will play an important role in the process of CO_2 dissolution. After a short introduction on the EoS in Chapter 2.1, in chapter 2.2 we will model the injection stage comparing our simulation to a model by Aavatsmark et al. [2]. The second model (chapter 2.3) will be related to the small scale dissolution trapping, associated with buoyancy-driven instabilities. This model setup is quite similar to the model investigated in [6]. However, in our study, the model is based on the Peng-Robinson EoS while in [6], the simplified description of the physics is used.

2.1. Equation of state

In this chapter, we will investigate the accuracy of the simulation results based on the Peng-Robinson EoS [16] with the ADGPRS simulator [20, 23]. As already mentioned in the introduction, all simulations in this study are based on the Peng-Robinson EoS. There are multiple different equations of state available, each with their own up- and downsides. Therefore we will briefly describe what equations of state there are and why it is necessary to use one for simulation of injection of CO_2 and impurities.

Equations of state are used to relate variables of gases and liquids such as pressure, volume and temperature to each other. One of the most known and simple equations of state is the ideal gas law:

$$pV = nRT \tag{2.1}$$

where p is the pressure of the gas, V is the volume, T is the temperature, n is the amount of moles and R is the ideal gas constant ($8.314 JK^{-1}mol^{-1}$).

The ideal gas law is useful to approximate the mentioned variables of gas in situations where gases behave like an 'ideal gas', which is a good approximation for gases under standard conditions. However, for reservoir conditions at higher pressure, the gases in the model will not behave like an ideal gas, as the volume estimated by the ideal gas law will be too low for the actual volume of the gas. For this reason, more extensive EoS are used.

More extensive EoS have been created to better approximate the behaviour of gases at higher pressure and temperature close to critical values. Those equations include Peng-Robinson (1976)[16], Redlich-Kwong (1949)[17] and Soave-Redlich-Kwong (1972)[19], which all are cubic EoS. For the purpose of approximating the real gas behavior, we need to introduce a compressibility factor, which is defined as the ratio between the volume of a real gas and the volume of an ideal gas $Z = V_{real}/V_{ideal}$. In this case, the compressibility factor can be found as:

$$Z = \frac{pV}{nRT} \tag{2.2}$$

The cubic Equation of State mentioned above can be generalized in the following form:

$$Z^3 + E_2 Z^2 + E_1 Z + E_0 = 0 \tag{2.3}$$

where $E_2 = (m_1 + m_2 - 1)B - 1$, $E_1 = A + m_1 m_2 B^2 - (m_1 + m_2)B(B+1)$ and $E_0 = -(AB + m_1 m_2 B^2 (B+1))$. The difference between the various cubic EoS is the values which are used for m_1, m_2, A and B. For example, SRK uses $m_1 = 0, m_2 = 1$ and Peng-Robinson uses $m_1 = 1 + \sqrt{2}, m_2 = 1 - \sqrt{2}$, which for PR results in the equation:

$$Z^3 - (1-B)Z^2 + (A - 2B - 3B^2)Z - (AB - B^2 - B^3) = 0 \tag{2.4}$$

For more information about the generalized version of cubic EoS, please refer to [8].

A recent paper from Aavatsmark et al. [2] suggests a generalized cubic equation of state for more accurate density calculations for application to pure CO_2 injection in aquifers. The paper suggests alternative parameters created especially to better fit data of CO_2 dissolution in water. In the next section, we will compare the PR EoS with the standard and newly proposed parameters, and make a choice for our simulations of CO_2 injection with impurities.

2.2. Injection stage of CO_2 sequestration

As a first example of the CO_2 sequestration process, we compare the CO_2 distribution results based on the classic PR EoS with simulation results reported in [2]. We perform a simulation using the Automatic Differentiation General Purpose Research Simulator (ADGPRS) developed at Stanford [20, 24]. We implemented a correction of the EoS coefficients proposed in [2] in order to compare them with classic results. However, the suggested corrections led to the divergence of the simulation process in the range of parameters we used for the simulation. Even for the parameters which let us perform separate flash calculations, the EoS iterations with adjusted parameters could not converge for the mixtures with impurities. That is why we decided to only compare simulation results, reported in [2] and simulation results with the convenient parameters of PR EoS performed in ADGPRS.

For our simulation model, we used the conditions reported in [2] for an appropriate comparison:

- 50 high by 50 wide gridblocks
- Grid size of 10m high, wide and deep (dx = dz = 10m) for a 500m by 500m reservoir
- Depth of the top of the reservoir = 500m
- Pressure in the model = Hydrostatic
- Entry Pressure = 1kPa
- Temperature = 307 K (everywhere, isotherm)
- Porosity = 0.2
- Residual brine saturation = 0.2
- Residual gas saturation = 0.05
- Permeability = 1 Darcy
- EoS = PR (different from Aavatsmark)
- Initially entirely filled with only brine (density 1182 kg/m^3)

The results of simulation and comparison are shown in Fig. 2.1. The original example by Aavatsmark is shown at the right (b) and the result of our simulation at the left (a). In both models CO_2 gas is injected at the left side of the reservoir near the bottom between 880 and 920m deep. The gas slowly spreads as a part of it is residually trapped and the rest is moving upwards due to buoyancy.

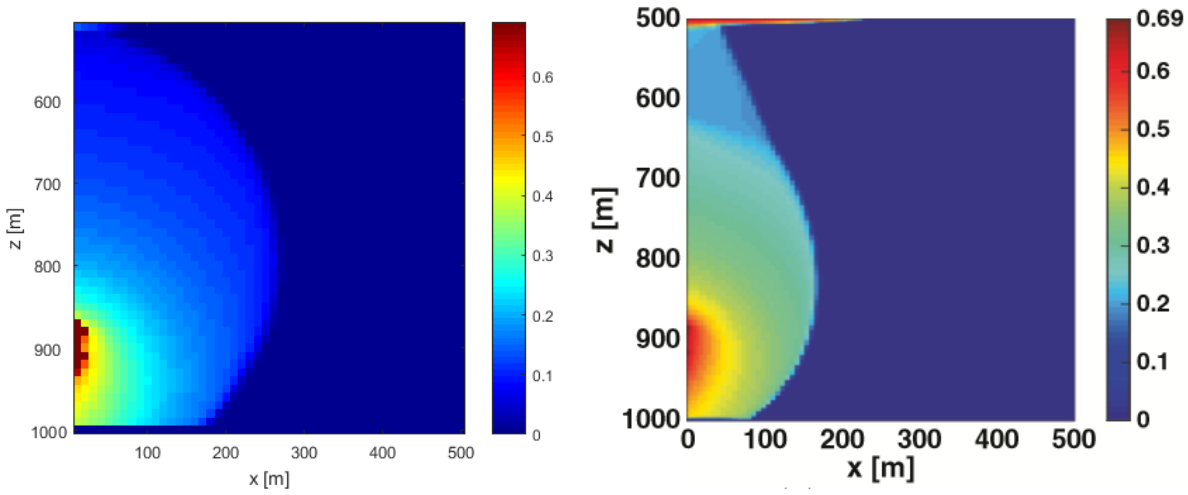

(a) ADGPRS simulation results

(b) Original results of simulation from [2]

Figure 2.1: Comparison between ADGPRS-based simulation of CO_2 saturation after 40 days of CO_2 injection with results from [2].

When comparing the results, they show a similar general trend of expansion of the CO_2 sideways and upwards. On the other hand, the spreading of CO_2 seems to be slightly faster in the Aavatsmark model due to adjusted EoS parameters. However, in general, we conclude that the difference is not very significant and both simulations yield sufficiently similar results. Given the fact that Aavatsmarks parameters are specifically made for CO_2 dissolution without the addition of impurity gases, which are central to our research, we have therefore chosen to base our further calculations on the PR EoS with the standard parameters.

2.3. Dissolution stage of CO_2 sequestration

The purpose of the next model is to get an illustration of CO_2 trapping dissolution into the brine at macroscopic scale and compare this with the results reported in [6]. The reservoir model used for this simulation has the following parameters, which are also true for all the following simulations, unless specified otherwise:

- 50 high by 50 wide gridblocks
- Grid size of 1m high and wide (dx = dz = 1m) for a 50m by 50m reservoir
- Depth of the top of the reservoir = 2475m
- Pressure = Hydrostatic
- Temperature = 356 K (everywhere, isotherm)
- Porosity = 0.15
- Permeability = 100 mD
- EoS = SRK
- Initially entirely filled with only brine (salt water, 1.1e3 kg/m^3) except top row of the grid, which is brine saturated with CO_2

Both diffusion and convection forces play an important role in this process. The diffusion controls CO_2 dissolution at an interface between saturated and unsaturated brine. In Fig. 2.2a. you can see an initial diffusion of CO_2 into the brine at the interface between saturated and unsaturated brine. Notice that no two-phase region is present in the model and the saturated CO_2 region is formed by a single-phase brine. Due to the higher density, the CO_2-rich brine starts the formation of unstable fingers, which is shown in Fig. 2.2b.

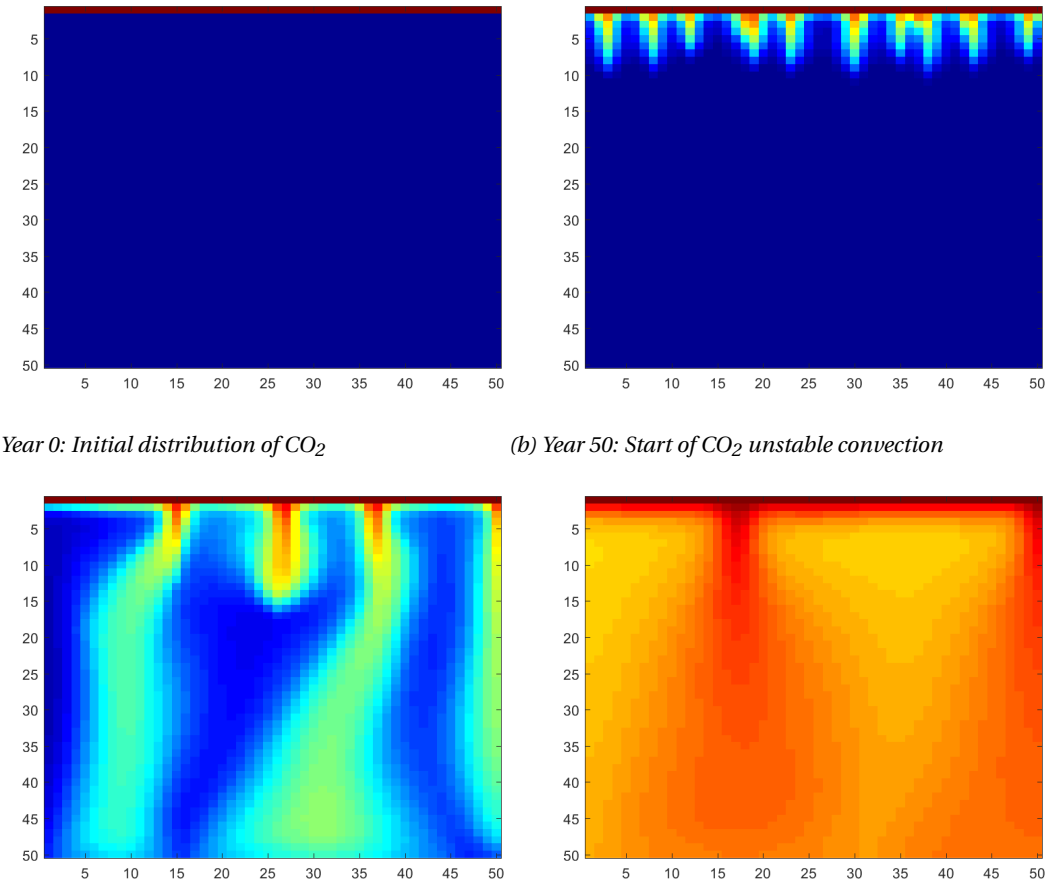

(a) Year 0: Initial distribution of CO_2

(b) Year 50: Start of CO_2 unstable convection

(c) Year 500: CO_2 fingers reach bottom

(d) Year 2400: brine almost entirely saturated with CO_2

Figure 2.2: The process of CO_2 dissolution in brine at different steps in time.

This process enhances the CO_2 dissolution due to a larger contact interface between CO_2-rich brine and fresh brine and this speeds up the CO_2 spread.

After 500 years, shown in Fig. 2.2c., the bottom of the model is reached mostly due to convection. After that point, convection becomes less dominant and the dissolution rate slows down until the domain is (almost) fully saturated with CO_2 as shown in Fig. 2.2d. This model has shown that the process of dissolved CO_2 spreading through water is characterized by two things: (a) the faster and nearly constant convection process of dissolved CO_2 flowing mostly downwards and (b) the slower and decreasing diffusion process of CO_2 moving towards lower concentrations, which is mostly sideways due to concentration differences as a result of the convection.

The resulting dissolution rate of CO_2 over time is shown in Fig. 2.3a. In this figure, the two time periods are easily distinguishable: before 500 years the gas dissolution rate stays relatively constant, while after 500 years the gas dissolution appears to go down in a straight line (apart from a small bump). Keep in mind that the graph has a log-log scale, so the dissolution rate does not go down linearly. This is in line with what you would expect from a diffusion process which directly depends on a decreasing concentration difference. For comparison, in Fig. 2.3b the macroscopic dissolution rate reported in [6], is shown. While the dynamic of both dissolution rates is similar, values in dissolution rate are different. That can be explained by the fact that our simulation only includes the single-phase macroscopic dissolution, whereas in [6] the influence of the static capillary transient zone is also included.

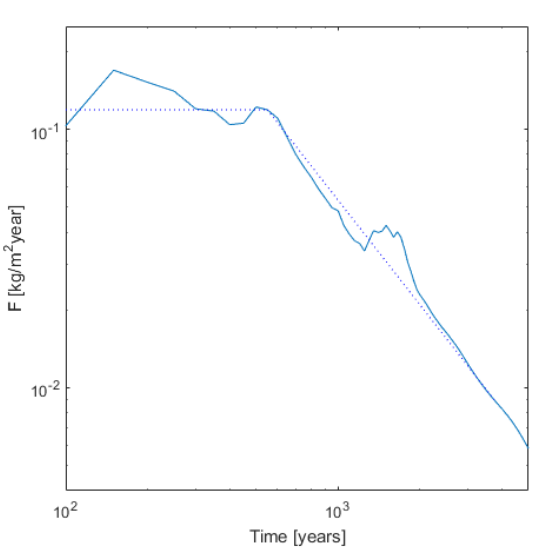

(a) Gas dissolution rate over time for single-phase flow

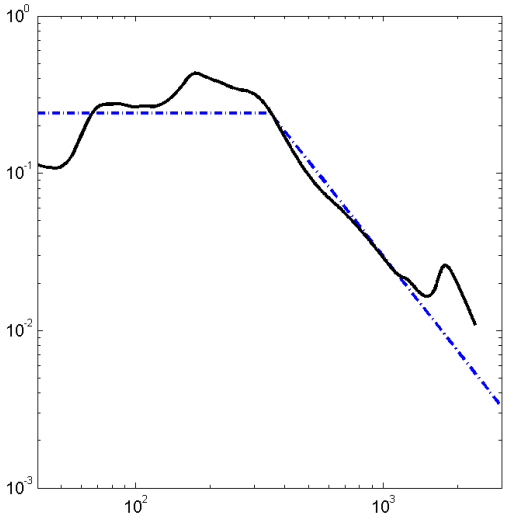

(b) Gas dissolution rate over time for static capillary transient zone, reported in [6]

Figure 2.3: The CO_2 dissolution rates (in log-log scale), a comparison of our simulation (a) to the result reported in [6] (b).

3

Large scale simulation

In this chapter, we will study the propagation of a large gas plume in an aquifer in case of a pure CO_2 stream and CO_2 streams with impurities - H_2S and CH_4.

3.1. Propagation of a pure CO_2 plume

Here we look into the process of plume propagation in the large scale domain with pure CO_2 in the injected gas stream. Our model is a 2D idealized version of the aquifer shown in Fig. 1.1. The modeled aquifer is 5 km wide and 50 m high, filled with brine (salt water) and tilted by 1%, so the right side is 50 m higher than the left side. The grid resolution is 20 m wide and 1 m high. Initially, there is a column of undissolved CO_2 gas in brine of 600 m wide along the left side of this model, to represent the idealized post-injection CO_2 distribution. As the simulation starts, this body of gas will at first move upwards and then move along the top of the reservoir towards the higher right side of the model. Along the way, the gas will slowly dissolve in the water, and after the onset time [6], the dissolved CO_2 starts forming unstable fingers and sinks to the bottom of the reservoir.

The results of the simulation with pure CO_2 are shown in Fig. 3.1 and 3.2. The first figure shows the movement of the gas saturation (red) as it goes upwards and then sideways through the water (blue), while leaving behind residually trapped gas (light blue). Notable is the decrease in size of the gas plume as a result of gas dissolution. Fig. 3.2 shows the concentration of CO_2 in brine at the same time steps. Notable here is the process of dissolved CO_2 leaking down from the location of the gas plume, just like the process shown in the previous chapter.

Similarly to [6], the density of brine increases by up to 1% when CO_2 dissolves in it, which causes gravitational instabilities where fingers of denser brine move downward while undersaturated brine moves upward to replace it. This process greatly enhances the dissolution process compared to pure diffusive transport of dissolved CO_2. However, in our simulation, we use the full EoS description, which can let us account for various impurities in the gas stream. In order to quantify the macro-scale CO_2 dissolution below the plume, we define a control region far to the right from the initial CO_2 column and below the region exposed to the saturated part of the CO_2 plume. The chosen control region is 400 m wide and 35 m high, starts at the bottom and 3600 m to the right and is indicated by black lines in Fig. 3.3, which also shows a magnified version of this region. Since the main direction of dissolved CO_2 is downwards and both the sideways movement of diffusion near the column and the sideways movement of the gas plume at the top are avoided, we can now assume that all of the dissolved CO_2 is entering the control region through the upper boundary. In the simulation process, we will account for the CO_2 dissolved in this region.

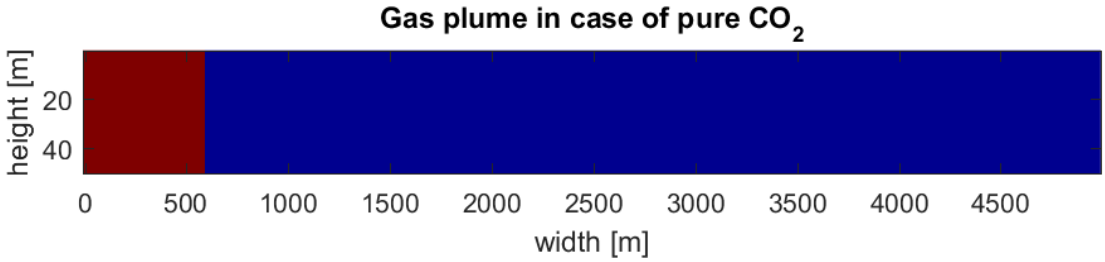

(a) Year 0

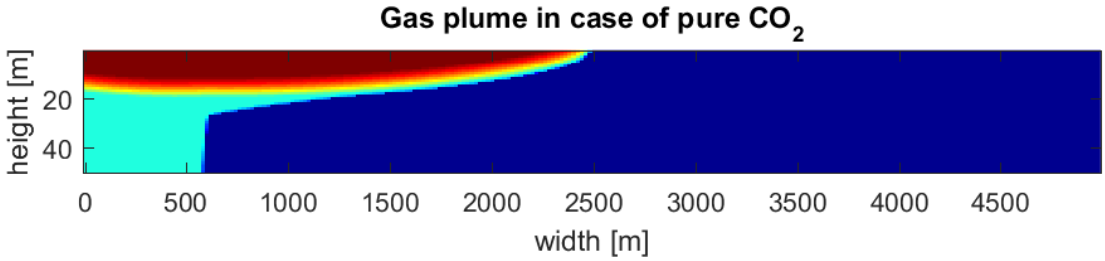

(b) Year 500

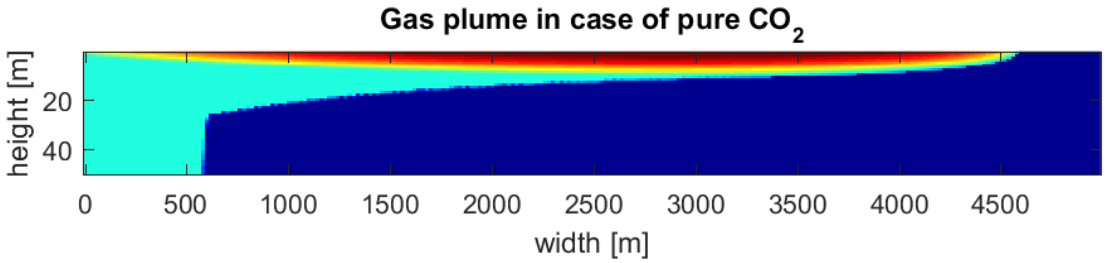

(c) Year 2000

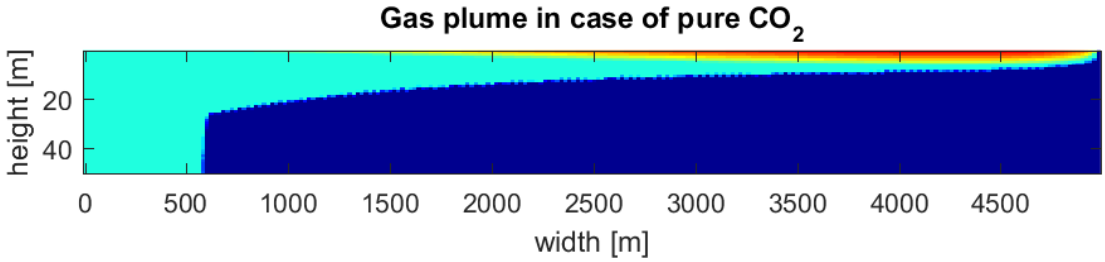

(d) Year 4000

Figure 3.1: CO_2 gas in the reservoir over time

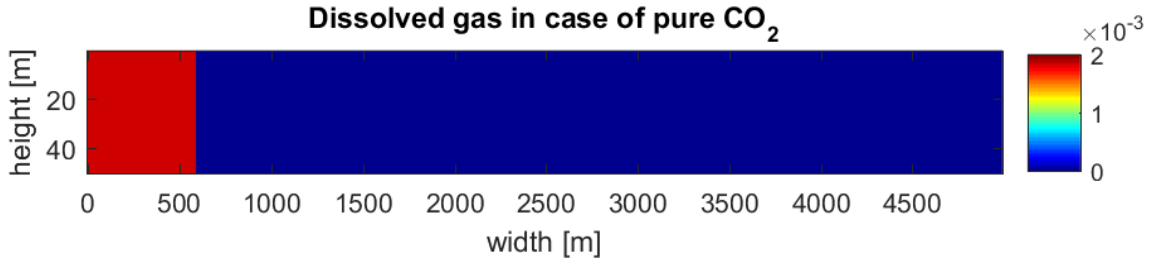

(a) Year 0

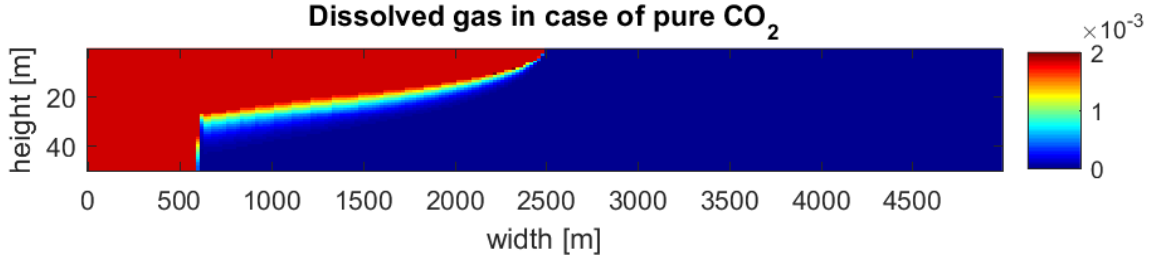

(b) Year 500

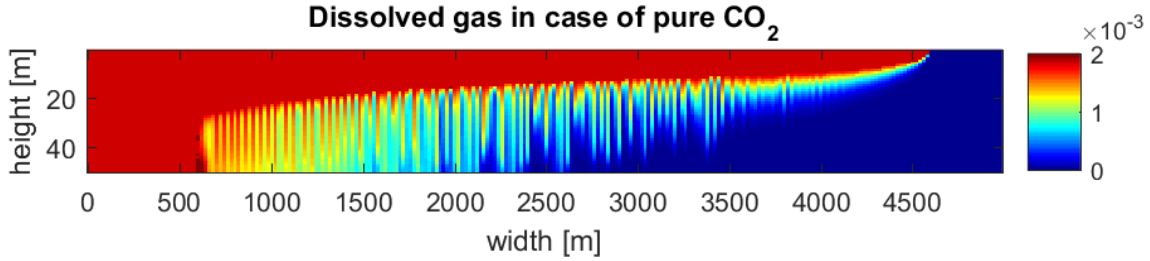

(c) Year 2000

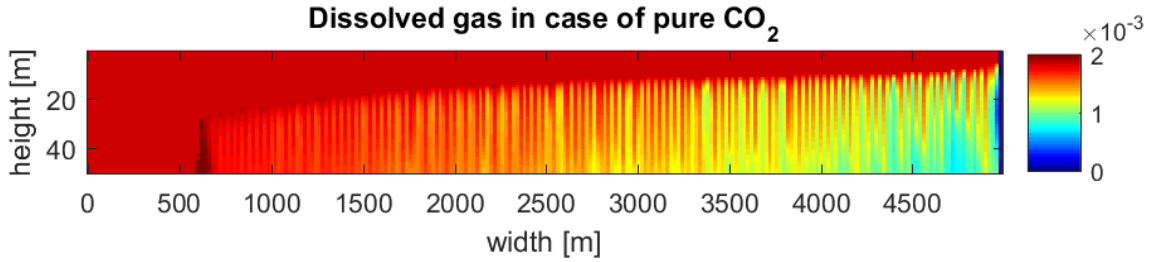

(d) Year 4000

Figure 3.2: Large scale low res reservoir, Dissolved CO_2 over time

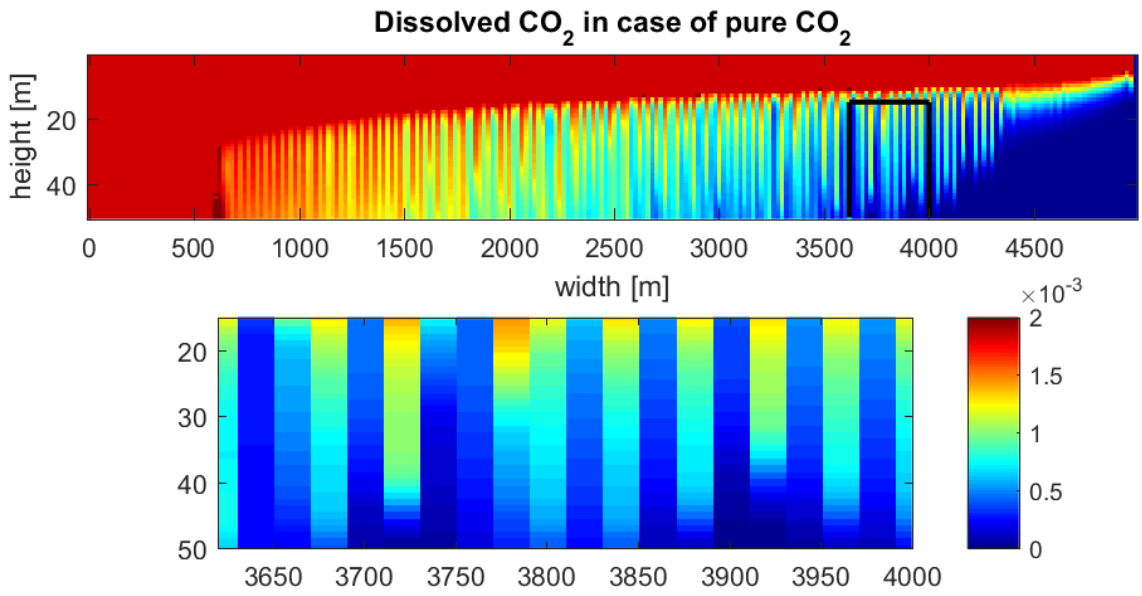

Figure 3.3: A larger version of Fig. 3.2 at 2500 years. The region within the black lines is magnified at the bottom to better show the dissolved CO_2 sinking through the water.

3.2. Plume propagation with impurities in gas stream

Now, that we created the model to determine the dynamics of macro-scale CO_2 dissolution, the next step is to repeat the same simulation with the addition of impurities to study the effect of these gases on the dissolution process of CO_2. Two common impurities present in an anthropogenic CO_2 stream are methane (CH_4) and hydrogen sulfide (H_2S). These gases have quite different solubilities in comparison to CO_2: CH_4 is much less soluble in brine and H_2S is more soluble.

The first simulation was performed for a mixture of gases containing 90% CO_2 and 10% CH_4 (molar fractions), and in the second simulation, a mixture of 90% CO_2 and 10% H_2S was used as the injection stream. The resulting distribution of dissolved gas after 2500 years in all three cases is plotted in Fig. 3.4. For all three simulation runs, the amount of gas entering the control region over time is shown in in Fig. 3.6. From these results, the mass flux (flow rate per unit area) of gas in all three cases can be derived, which is plotted in Fig. 3.7.

There are several interesting details to notice in Fig. 3.4, Fig. 3.6 and Fig. 3.7. In Fig. 3.4, we see an effect of accelerating gas dissolution in case of CH_4 (fingers formed and progressing down faster), while there is not much of a difference visible between pure CO_2 and a mixture of CO_2 with H_2S. For completeness, in Fig. 3.5, the distribution of the dissolved impurities in the previous simulations is shown apart. The color scale of H_2S is the same as the previous figures. For the sake of visibility, the color scale of the distribution of CH_4 has been changed and is two orders of magnitude lower than the colour scale of all other figures. Nevertheless, this figure is showing mostly shades of blue, which indicates a very slow CH_4 dissolution rate. H_2S appears to follow the same distribution pattern as CO_2, but at a slightly lower rate. An interesting thing to notice is that the amount of dissolved H_2S appears to decline towards the tip of the plume.

Fig. 3.6 and Fig. 3.7 demonstrate that the gas plume with CH_4 enters in the control region much earlier than in other cases. The fast arrival of CH_4 is explained by the significantly lighter weight of CH_4 gas (16 g/mole, compared to 44 g/mole of CO_2 and 34 g/mole for H_2S), which results in a higher velocity of the lighter gas plume partly consisting of CH_4. The differences in velocity of the gas plumes are shown in Fig. 3.8 where the gas plume in all three cases is plotted at the same time after 1000 years. As a consequence, the slightly lighter gas fingers with CH_4 arrive faster into the control region.

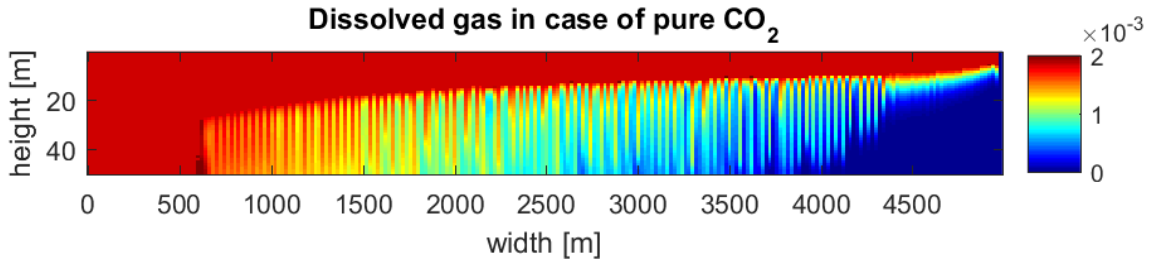

(a) Dissolved CO_2 in case of pure CO_2

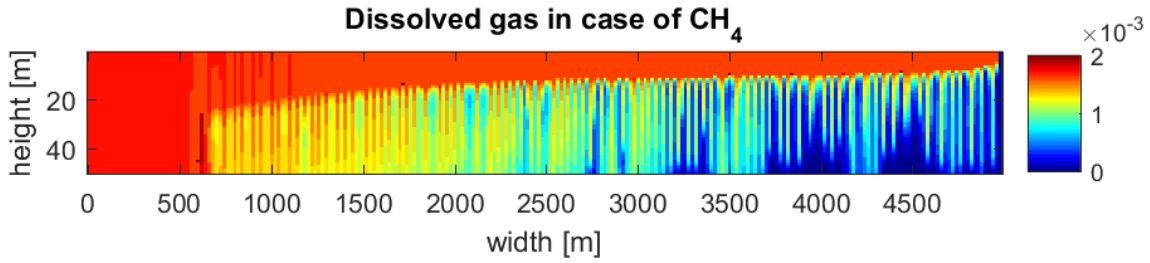

(b) Dissolved total gas in case of CH_4

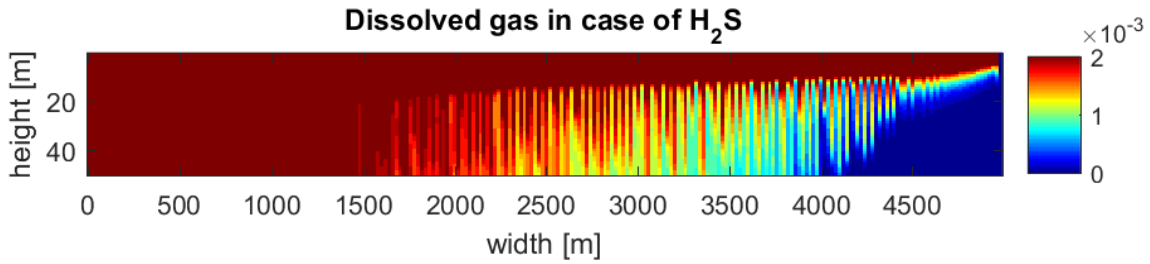

(c) Dissolved total gas in case of H_2S

Figure 3.4: Large scale low res reservoir, dissolved CO_2 after 2500 years in three cases

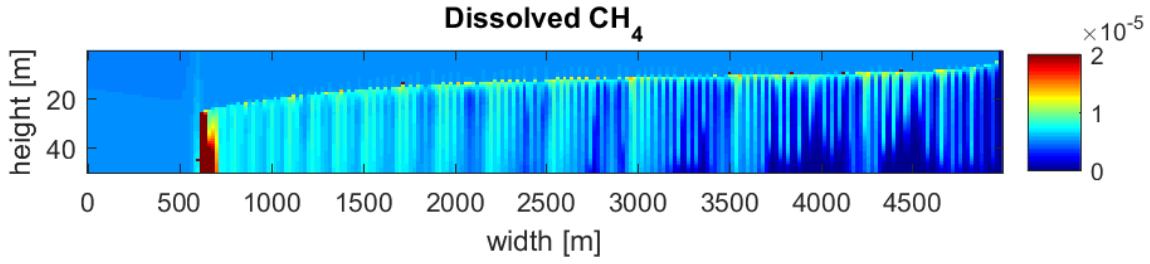

(a) Dissolved CH_4 (Notice different colour scale to make the dissolution visible, CH_4 dissolves much less than the other two gases)

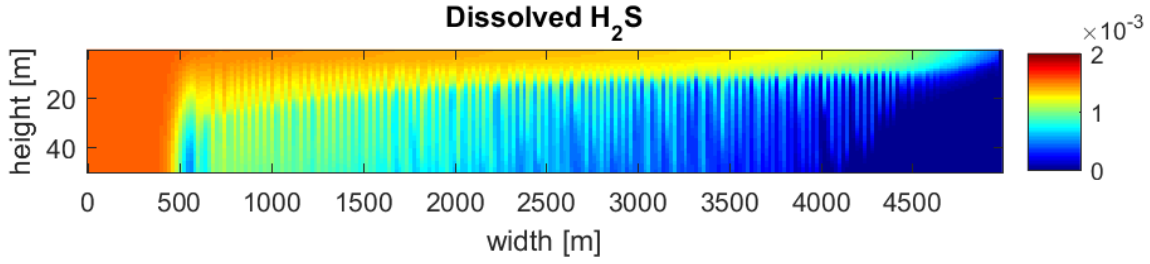

(b) Dissolved H_2S (Same colour scale as all the previous figures, except Fig. 3.5 (a))

Figure 3.5: Large scale low res reservoir, dissolved impurity gases after 2500 years

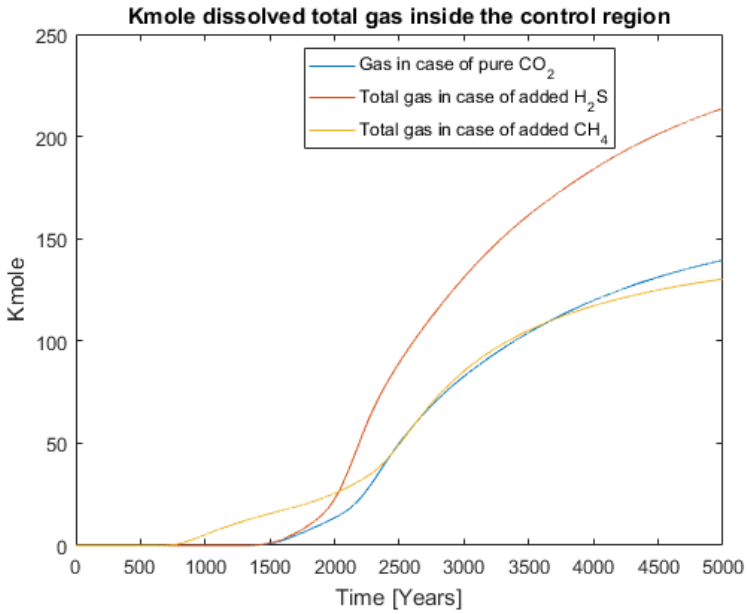

Figure 3.6: Large scale, low resolution: dissolved CO_2 in the control region as function of time

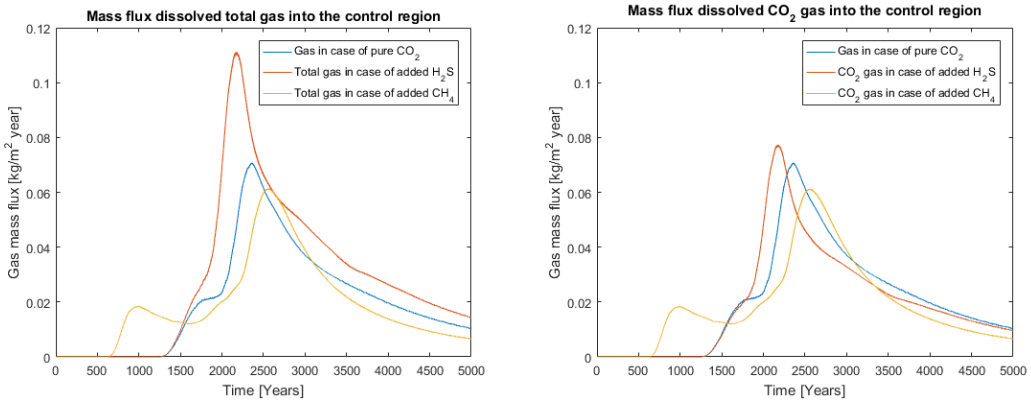

(a) Dissolved total gas *(b) Dissolved CO_2*

Figure 3.7: Large scale, low resolution: Total gas mass flux (left) and CO_2 mass flux (right) into the control region

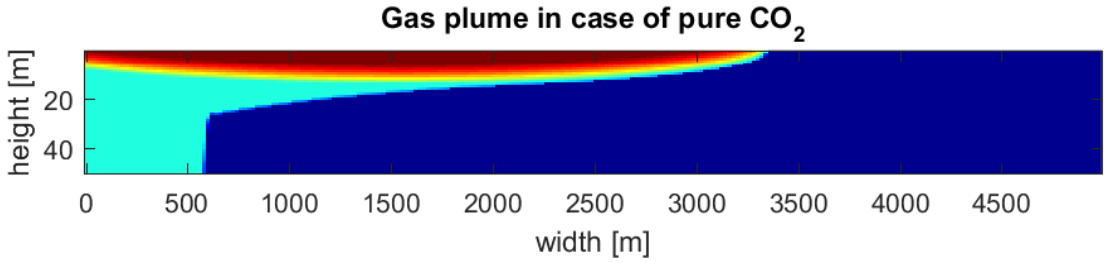

(a) Gas plume pure CO2

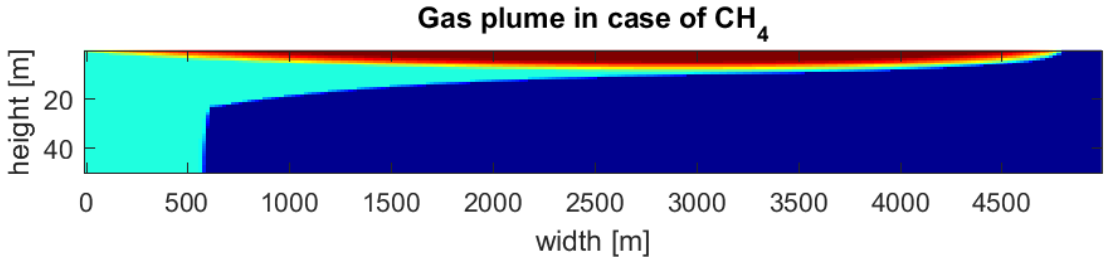

(b) Gas plume with C1

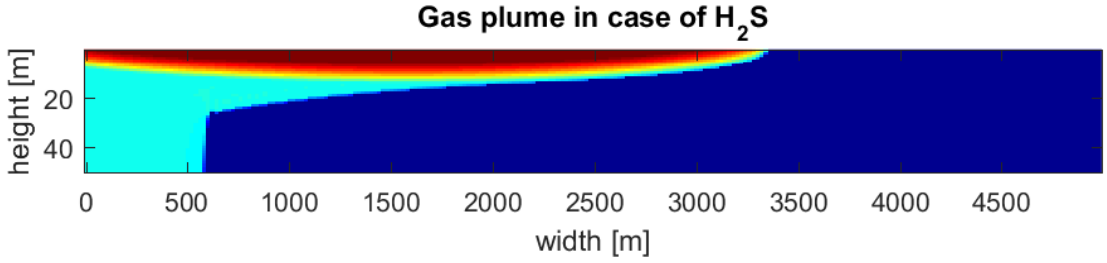

(c) Gas plume with H2S

Figure 3.8: Large scale low res reservoir, Gas plume after 1000 years in three cases: pure CO2, CO2 with 10% C1 impurity and CO2 with 10% H2S. Notice the large difference in case of C1.

Table 3.1: Large scale, low resolution: Peak mass flux

Situation	CO_2 mass flux $[kg/m^2 year]$	Total gas mass flux $[kg/m^2 year]$
Pure CO_2	0.071	(same)
In case of CH_4	0.061	0.061
In case of H_2S	0.077	0.111

In Table 3.1 the peak mass flux is shown for every graph in Fig. 3.7. These values will be useful in the next chapter, where they will be compared to similar peak mass flux values of a different simulation. Note that the reported dissolution rate corresponds to a low resolution simulation. It is possible to perform a convergence study similar to one described in [6] for the case of impurities. However, this solution will require enormous simulation time since we need to deal with a large compositional system based on equation of state. Instead, we decided to apply correction factors to the low resolution results which will be described in the next chapter.

To conclude this chapter, we can say that the model can capture an important difference between the dissolution of a CO_2 stream with or without impurities. The introduced control region makes it possible to determine the macroscopic dissolution rate of gas mixtures. We can clearly designate the different behaviour for all three types of streams in our simulation: pure CO_2 and two mixtures of CO_2 with CH_4 and H_2S. We noticed that the resolution of this large scale model is rather low and it may require specific correction to capture the influence of impurity to the gas dissolution rate accurately enough. The convection process shows quite complex dynamics of the dissolved gas as it moves downwards, which can be seen in the figures in Chapter 2 with a higher resolution. These effects seem to be missing in the region used for computation of the dissolution rate shown in Fig. 3.3.

4

Accurate evaluation of macroscopic dissolution

In the previous chapter, we have looked at a 5 km wide reservoir and estimated the macroscopic dissolution rate using a control region of 400×35 m wide. In this chapter, we will evaluate the dissolution rate using a small scale model, similar to the control region in the previous chapter. However, two things will be significantly different in this model: the boundary conditions for the CO_2 source and the simulation accuracy of the CO_2 convection process.

4.1. Low resolution model

First, we are going to study the effect of boundary conditions on the results of the macroscopic dissolution rate evaluation. The total size of the simulation domain in this model model is 400×50 m. Inside of this model, we again define a control region equivalent to the size of the control region of the large scale model from the previous chapter, which is equal to (400×35 m). We use the same resolution of 20×1 m per gridblock.

To provide the source of gas, we define a large volume of the domain in the upper gridblock, which is filled with brine fully saturated with gas. This source is very different from the boundary conditions imposed by the real plume and studied in the previous chapter. The effective difference between this rate and the rate evaluated in the previous chapter allows us to estimate the influence of the boundary conditions on the results obtained from the small scale model. In total, we are going to model three scenarios, similar to the test cases in the previous chapter: pure CO_2, and a mix of CO_2 with either 10% H_2S or CH_4.

The results of the small scale simulation are plotted in Fig. 4.1 and Fig. 4.2. The first figure shows the amount of gas entering the control volume over time, from which the mass flux of gas is derived and plotted in the next figure. As can be seen in Fig. 4.2 there are three distinct periods in time in the process of gas dissolution in the control region, and all of them can be recognized in all three curves.

In the first period, we see a weak linear increase in time when the first portion of unstable fingers is reaching the control region. At the beginning of the second period, we see a large jump in dissolution rate when all fingers have reached the control region and enhanced the dissolution inside it. After the peak in dissolution rate has been reached, there is a rapid decay in the rate related to fingers reaching the bottom of the domain. At this point, most of the brine contains some dissolved gas, but it is not fully saturated yet. Finally, the decay with a lower angle corresponds to a reduction in dissolution rate due to a gradual saturation of the control region.

Some interesting observations can be made from Fig. 4.2 when comparing it to the equivalent figures (Fig. 3.7) from the previous chapter. At start, the general shape of the CO_2 and total gas mass flux over time is very similar and contains the three distinct periods mentioned earlier: startup, peak and decay. Next, the height of the peaks is almost the same: between 0.06 and 0.08 $kg/m^2 year$ and highest in the case of impurity gas

Table 4.1: Small scale, low resolution: Peak mass flux

Situation	CO_2 mass flux $[kg/m^2 year]$	Total gas mass flux $[kg/m^2 year]$
Pure CO_2	0.083	(same)
In case of CH_4	0.062	0.064
In case of H_2S	0.084	0.100

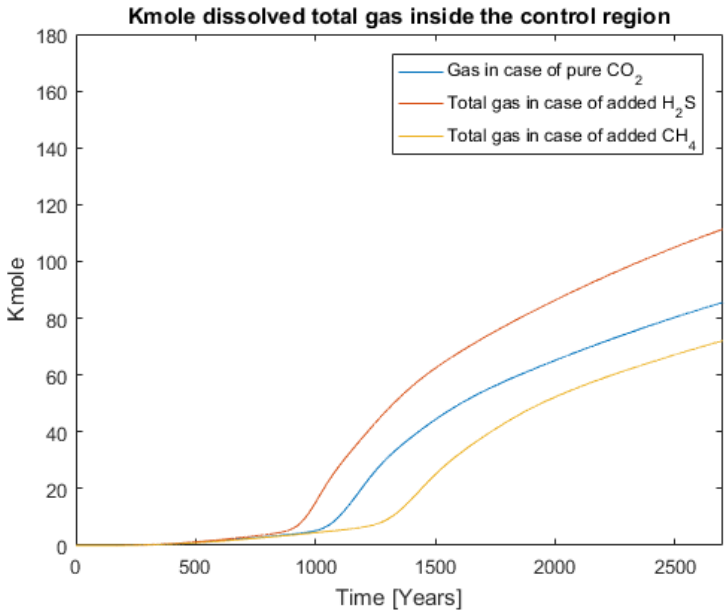

Figure 4.1: Small scale, low resolution: dissolved CO_2 in the control volume as function of time

H_2S and pure CO_2, lowest in case of impurity gas CH_4.

Now we go on to the differences: one small difference with the large model is that the height of the peak in case of pure CO_2 is equal to that of the peak in case of 10% H_2S in the small model, while it was halfway in between the highest and lowest peak in the large model. The main difference with the large model is the shorter duration of the first period where the fingers of dissolved gas have not yet reached the control volume. This is caused by the fact that there is no gas column to move up and sideways in the small model, which explains the faster arrival of the peaks in Fig. 4.2. Another difference is that the gas in case of CH_4 arrives much later in the small scale model: it arrives after the other two scenarios instead of before, as it did in the large model. In the previous chapter, we have explained that the gas in case of CH_4 arrives much faster, because of the faster propagation of the plume tip, which is obviously not present in the small model. The fact that the dissolution with CH_4 is slower in comparison to the other two scenarios is a new observation.

The mass flux peak values are shown in Table 4.1 and while they are similar to the ones shown in Table 3.1, they are mostly a bit higher, except for the total gas mass flux in case of H_2S, which is a bit lower. These differences are a result of the different boundary conditions and we will later use the ratio between these rates as a correction factor between the rate obtained from the small scale model and the rate related to the large scale macroscopic dissolution. Leaving the different timing of the arrival of the gases aside, we believe that the ratio between the two coarse scale models will address correctly the difference between the idealized boundary conditions of the small scale model and the realistic conditions of the large scale model. Next, we need to use a finer resolution in the small scale simulation model and obtain a converged solution for CO_2 with impurities, similar to [6].

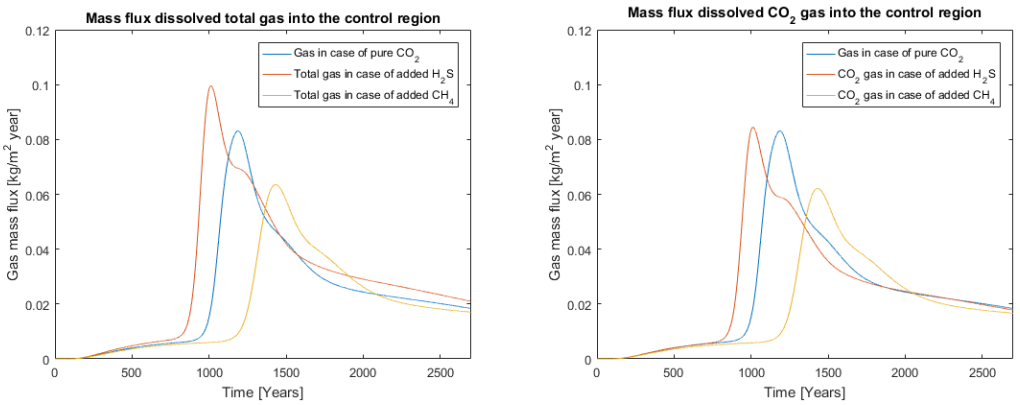

(a) Dissolved total gas *(b) Dissolved CO_2*

Figure 4.2: Small scale, low resolution: Total gas mass flux (left) and CO_2 mass flux (right) into the control region

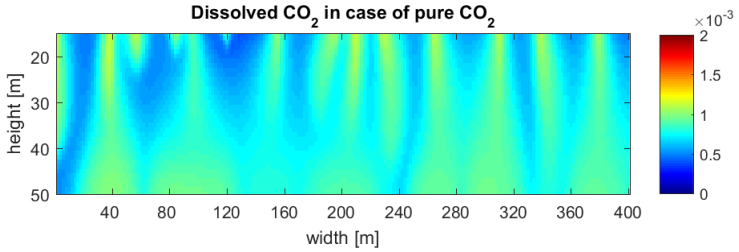

Figure 4.3: Small scale, high resolution: Dissolved CO_2 in the reservoir after 500 years.

4.2. Converged dissolution rate

In this section, we are going to evaluate high resolution results for the macroscopic dissolution rate. A benefit of the smaller scale model is that the lower calculation time allows for a higher resolution and more accurate results. Even though the main movement direction of the dissolved CO_2 is vertical due to the gravity, there are relevant sideways movements in the convection process as demonstrated in [18]. However, it is not possible to resolve this convective flow within the the coarse grid blocks. Therefore, we repeat the previous simulations, but now with grid blocks of 2 m wide and 1 m high, which is enough to capture the correct dissolution rate as shown in [6] for pure CO_2. In comparison, this small scale simulation has only taken a few hours, when modeling a large scale simulation as shown in the previous chapter, would have taken much more time (up to several months) at this resolution and complexity.

The resulting dissolution process is shown in figures 4.3 to 4.7. The first figure shows the spread of the CO_2 in the reservoir which reflects the expected pattern of CO_2 moving down, but much more detailed than the earlier low resolution model. In addition, the movement of dissolved gas is not entirely vertical and includes convective deviations. Fig. 4.4 and Fig. 4.5 show a similar pattern for the cases with added impurity gases CH_4 and H_2S. The last two figures 4.6 and 4.7 are quite similar to Fig. 4.1 and 4.2; however, the peaks in dissolution rate are more irregular (they show multiple sub-peaks). The second period, when the dissolution rate inclines faster, arrives 500 years earlier in all three models. Both of these effects can be explained by the higher resolution and larger influence of instability.

The irregular form of the peaks is a result of a greater visibility of the interplay between the gravity fingers, where they fuse together or spread sideways before reaching the bottom. These processes can only be resolved at a higher resolution when all unstable convection is described more accurately. The faster arrival of the gas is also the result of a more accurate simulation. Convection of CO_2-saturated water is much faster than diffusion of CO_2, but a lower resolution model does not allow for it to be resolved properly.

Since there is no clear peak value at this higher resolution, we have chosen to calculate average peak values, which are shown in Table 4.2. These values can be compared to those in Table 3.1 and 4.1. As we can see,

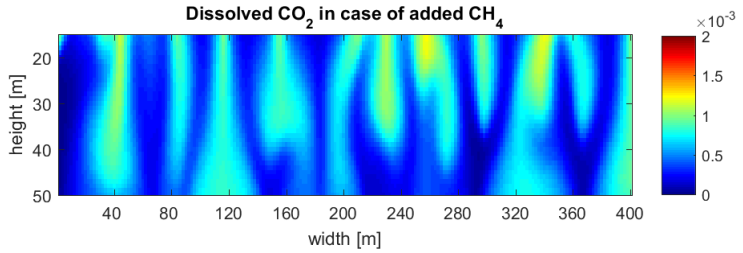

Figure 4.4: Small scale, high resolution: Dissolved CO_2 in case of C1 in the reservoir after 500 years.

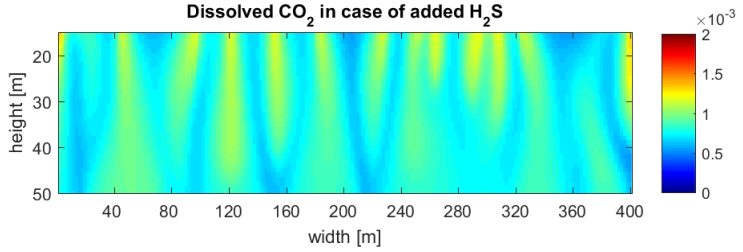

Figure 4.5: Small scale, high resolution: Dissolved CO_2 in case of H_2 in the reservoir after 500 years.

these average peak values of Table 4.2 are slightly lower, as we would expect from an average taken from the top of the curve instead of the maximum value.

These average peak values are also shown as dotted lines in Fig. 4.8, where the three mass flux graphs of Fig. 4.7 are individually shown with their respective average peak value in a logarithmic scale. Also shown is a second dotted line which represents the general trend in the decline phase after the last peak; these lines of the form $F = a * t^b$ appear as straight lines in the log-log scale.

To conclude, the higher resolution shows more accurately the dynamics of the dissolution process than the simulations at a lower resolution.

4.3. Correction of the small scale rates

As we mentioned in the beginning of this chapter, the high resolution simulations of a small scale model should predict the macroscopic dissolution rate quite accurately. However, the boundary conditions, introduced at the upper boundary of the small scale model, will not accurately represent a realistic gas rate in the control region below the plume. That is why we first simulated the small scale model at a coarse rate equivalent to the resolution of our large scale model. This comparison helps us to estimate the differences in the dissolution rates caused by changing the boundary conditions. We can use these ratios between the peak values shown in Table 4.1 and Table 3.1 to correct the average dissolution rates obtained from the small scale simulation at high resolution. These correction factors are shown in Table 4.3.

One of these factors in Table 4.3 is slightly different than the others, the correction factor for H_2S for the total gas case is bigger than 1, while all the others are smaller. This difference can be explained by an effect that happens in the gas plume in the large aquifer model of chapter 3. One assumption we made was that the ratio of gases supplied in the small model is the same as the ratio of gases supplied by the gas column

Table 4.2: Small scale, high resolution: Average peak mass flux

Situation	Total gas mass flux $[kg/m^2 year]$
Pure CO_2	0.073
In case of CH_4	0.051
In case of H_2S	0.090

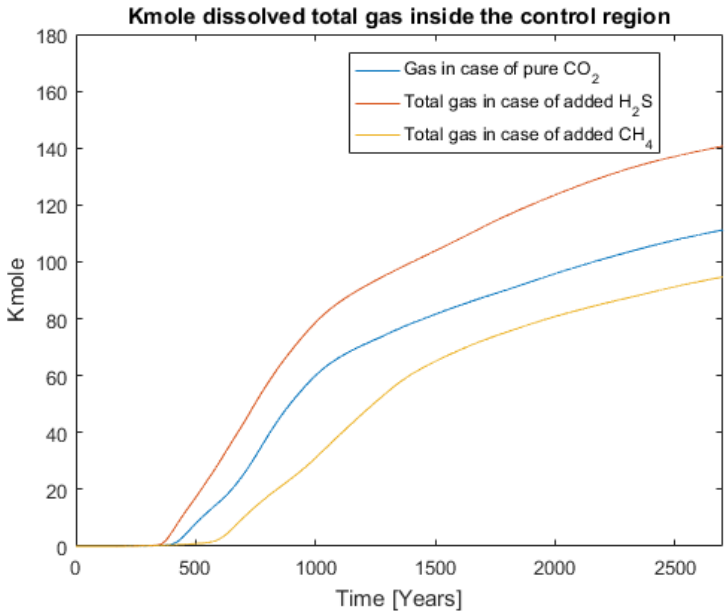

Figure 4.6: Small scale, high resolution: dissolved CO_2 in the control volume as a function of time

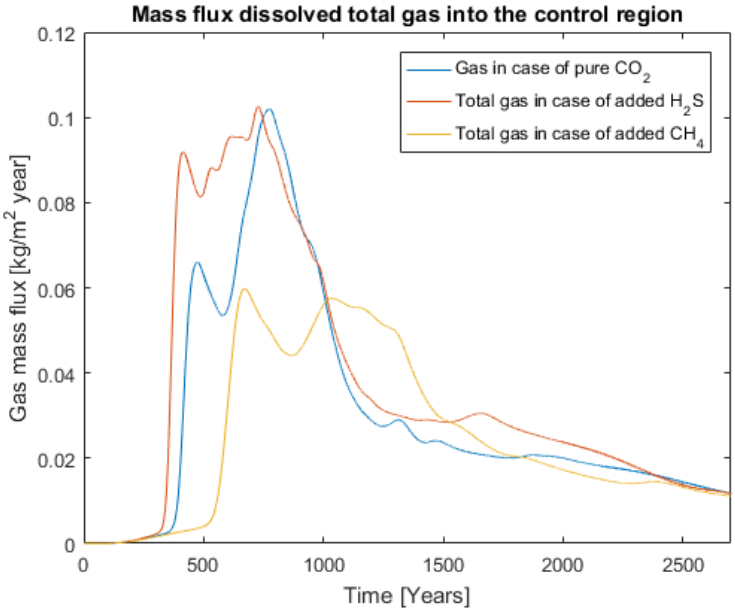

Figure 4.7: Small scale, high resolution: CO_2 mass flux into the control volume

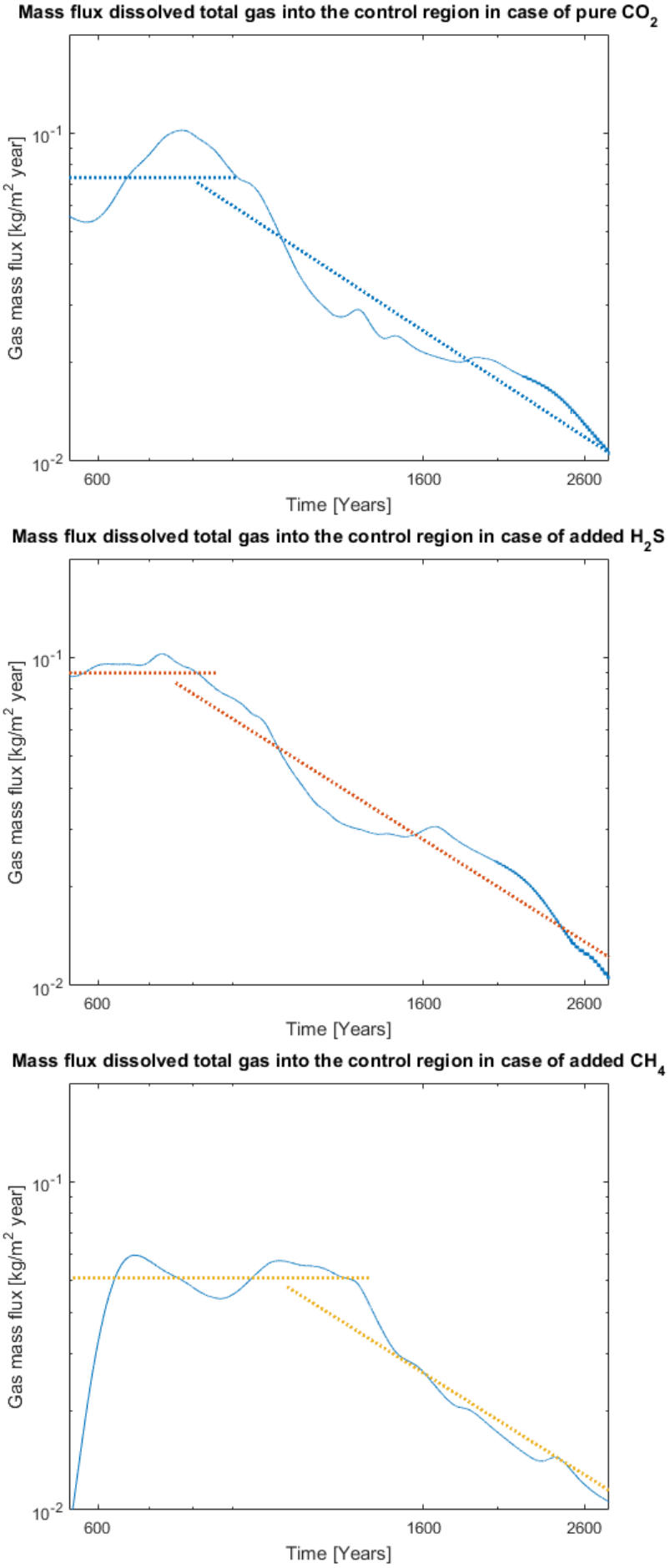

Figure 4.8: Individual cases of Fig. 4.7 shown with a horizontal line indicating the average peak mass flux and a line fitted to the decay region after the last peak.

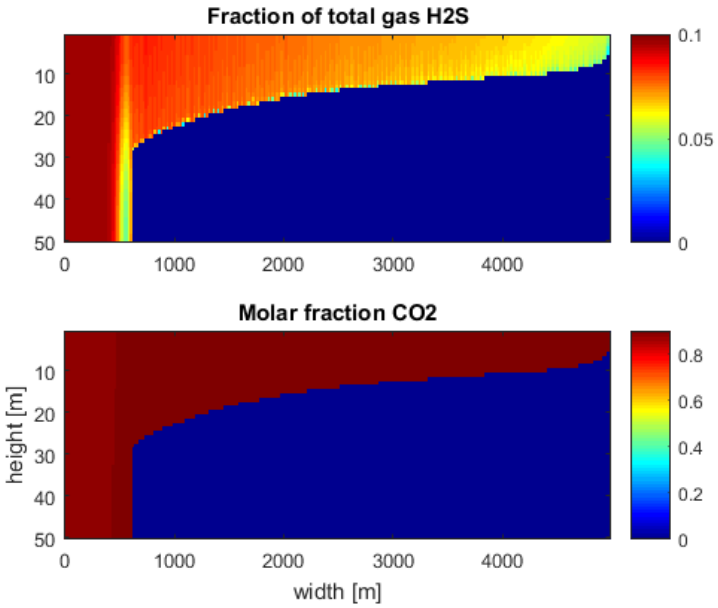

Figure 4.9: Large scale, low resolution: the molar fractions of H_2S and CO_2 in the gas plume are not constant.

Table 4.3: Correction factors to account for boundary conditions and resolution

Multiply rates of the small model by:	For CO_2 rate	For total gas rate
Pure CO_2	0.85	(same)
In case of CH_4	0.99	0.97
In case of H_2S	0.92	1.12

in the large model, namely 1:9 of impurity gas versus CO_2. However, it turns out that the gas ratio inside the gas column is not distributed evenly as the gas plume moves towards the right side of the aquifer in the large scale model presented in the chapter 3.

Due to the high solubility of H_2S, a significant amount of the the relatively small amount of H_2S leaks away from the gas plume as it dissolves into the water faster than CO_2. This process is shown in Fig. 4.9, where the fraction of H_2S and CO_2 to the total amount of undissolved gas is shown for the time where the right side of the aquifer is reached by the gas. Clearly visible is the fact that at the right side of the aquifer, the ratio of impurity to CO_2 is much less than 1:9, more in the order of 1:18. In Fig. 4.10, the similar distribution is shown for CH_4. This figure shows no significant change in ratio, because of the lower solubility and amount of CH_4 compared to CO_2. If the ratio of CH_4 to CO_2 were substantially different, we might expect to see a divergent effect in Fig. 4.10 as well.

In conclusion, the small model can be considered to be representative for the same situation in the large model, provided the correction factors of Table 4.3 are applied. Using these factors, we can correct the dissolution rates of Fig. 4.7, the result of which is shown in Fig. 4.11.

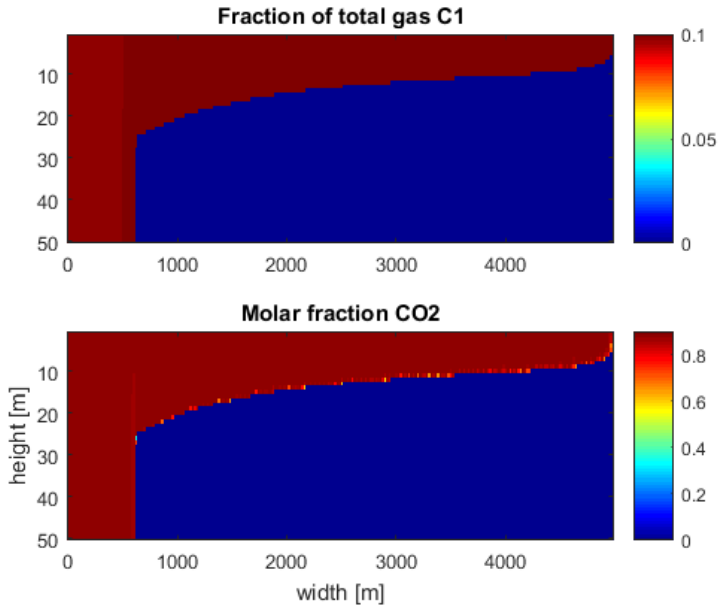

Figure 4.10: Large scale, low resolution: the molar fractions of CH_4 and CO_2 in the gas plume are (nearly) constant.

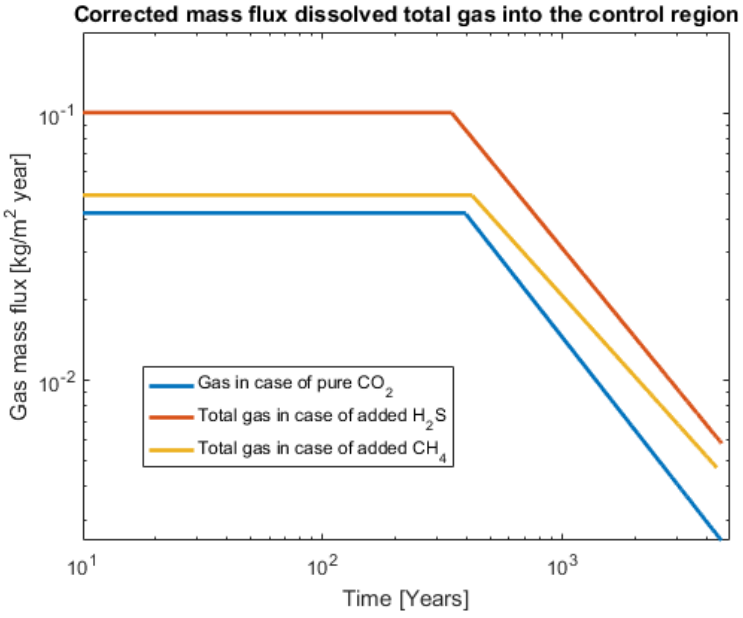

Figure 4.11: The total gas mass flux of Fig. 4.7 corrected by the factors of Tab. 4.3.

5

Summary and conclusions

The objective of this research was to determine the impact of impurity gases in CO_2 on the process of CO_2 dissolution in an aquifer. The chapter one describes the context of the research and in particular the relevance of CO_2 storage as one of the methods for a reduction of the CO_2 in the air in the face of the climate problem.

In the chapter two, attention is given to the various existing equations of state, such as the simple ideal gas law, Peng-Robinson and Soave-Redlich-Kwong. Two different regimes are modeled. The first deals with the injection stage and is based on a more recent EoS by Aavatsmark et al [2]. The second model is set up similar to a model by Elenius et al. [6] and concerns the small scale dissolution trapping, associated with a buoyancy-driven instabilities. Where Elenius et al. do not use EoS, our results were more or less convergent with their model. Therefore, we decided to continue our simulations with the PR EoS which is more convenient when impurities are present.

The third chapter finally touches the main objective of this paper and shows a simulation of CO_2 dissolving in a large tilted 50m high and 5km wide aquifer, where the gas column initially at the left starts by moving up due to buoyancy and then continues moving to the right side of the model along the top. From this gas column, the CO_2 dissolves into the water and moves down according to the process shown earlier in chapter two. To determine the rate at which CO_2 dissolves and moves in a mostly vertical movement down from the gas plume at the top, a control volume of 400m wide is defined in which the amount of CO_2 over time is measured. This process is then repeated twice with 10% of CO_2 replaced by an impurity gas: once with CH_4 and one with H_2S respectively. These gases are chosen for their different solubilities in water: CH_4 is much less soluble than CO_2 and H_2S is much more soluble than CO_2. The resulting figures definitely show a difference between the three scenarios, but we miss the sideways movement of dissolved gas in the figures, which was present in the section 2.3.

In the section 4.1, we compared this result with the result obtained with the same 20m wide resolution, but now in the lower part (35m x 400m) of the small subsystem, in which the gas is supplied from an above layer located at the top of the 50m x 400m system, thus abandoning the flowing gas plume in the large system. This calculation took only 20 minutes as opposed to 11 hours to calculate the large system. As we would expect, there is considerable mutual agreement between the two models. However, we observe in both cases that CH_4 impedes the dissolution of CO_2 while the addition of H_2S does not show this prevention, or might have a small accelerating effect. In the section 4.2, we performed the same simulation, but with a higher resolution of 2m wide instead of 20m. The results of the simulation with higher resolution yields more accurate information about the dissolution process. The peaks appear less smooth and the figures show the convection process better: there is more sideways movement of the dissolved gas, which was not visible at lower resolutions. In the section 4.3, we raise the question whether this small model could be considered to be representative for the dissolution process in the large model. We find that the ratio of the gases in the aquifer in the chapter 3 is not constant as it moves towards the right. Specifically, in the case of H_2S part of the impurity gas dissolves before it reaches the column of the control volume. We have concluded that in general terms, the small scale high resolution model may be considered representative for the large model, provided

that adequate correction factors are applied. These correction factors compensate for the effect of boundary conditions of the small scale model.

Thus this small scale high resolution model has potential for the simulation of the CO_2 dissolution process with mixture of impurity gases in aquifers within reasonable calculation time and high accuracy.

Bibliography

[1] Study of mineral trapping of co2 and seal leakage mitigation. *Energy Procedia*, 63(Supplement C):5490 – 5494, 2014. ISSN 1876-6102. doi: https://doi.org/10.1016/j.egypro.2014.11.581. 12th International Conference on Greenhouse Gas Control Technologies, GHGT-12.

[2] I. Aavatsmark, B.K. Kometa, S.E. Gasda, T.H. Sandve, and H.M. Nilsen. A generalized cubic equation of state with application to pure co2 injection in aquifers. *Computational Geosciences*, 20(3):623–635, 2016. doi: 10.1007/s10596-015-9537-0.

[3] S. Bachu. Sequestration of co_2 in geological media: criteria and approach for site selection in response to climate change. *Energy Convers. Mgmt.*, 41:953–970, 2000.

[4] S. Bachu. Screening and ranking of sedimentary basins for sequestration of co_2 in geological media in response to climate change. *Environmental Geology*, 44(3):277–289, 2003.

[5] S. Bachu, W. D. Gunther, and E. H. Perkins. Aquifer disposal of CO_2: Hydrodynamic and mineral trapping. *Energy Convers. Mgmt.*, 35:269–279, 1994.

[6] M.T. Elenius, D.V. Voskov, and H.A. Tchelepi. Interactions between gravity currents and convective dissolution. *Advances in Water Resources*, 83:77–88, 2015. doi: 10.1016/j.advwatres.2015.05.006.

[7] F. M. Orr, Jr. CO_2 capture and storage: are we ready? *Energy & Environmental Science*, 2(5):449–458, 2009.

[8] GeoQuest Schlumberger. Eclipse reservoir simulator. *Technical description*, 2013.

[9] Carbon Science & Engineering Research Group. Carbon capture and sequestration, 2011. URL `http://co2.egi.utah.edu/`.

[10] M. Hesse, A. Riaz, and H. A. Tchelepi. Convective dissolution of co2 in saline aquifers. In *Geochimica ET. Cosmochimica Acta*, volume 71 of *15*, pages A401–A401. American Geophysical Union, Pergamon-Elsevier Science Ltd, Oxford, 2007.

[11] M. A. Hesse, Orr, F. M. Jr., and H. A. Tchelepi. Gravity currents with residual trapping. *Journal of Fluid Mechanics*, 611:35–60, 2008.

[12] S. T. Ide, K. Jessen, and F. M. Orr. Storage of co_2 in saline aquifers: Effects of gravity, viscous, and capillary forces on amount and timing of trapping. *International Journal Of Greenhouse Gas Control*, 1(4):481–491, 2007.

[13] F. M. Orr Jr. Onshore geologic storage of CO_2. *Science*, 325:1656–1658, September 25 2009.

[14] Johannes Lehmann, John Gaunt, and Marco Rondon. Bio-char sequestration in terrestrial ecosystems – a review. *Mitigation and Adaptation Strategies for Global Change*, 11(2):403–427, Mar 2006. ISSN 1573-1596. doi: 10.1007/s11027-005-9006-5.

[15] Intergovernmental Panel on Climate Change. *Special report on carbon capture and storage*. Cambridge Univ. Press, New York, 2005.

[16] D.-Y. Peng and D.B. Robinson. A new two-constant equation of state. *Industrial and Engineering Chemistry Fundamentals*, 15(1):59–64, 1976. doi: 10.1021/i160057a011.

[17] O. Redlich and J.N.S. Kwong. On the thermodynamics of solutions. v. an equation of state. fugacities of gaseous solutions. *Chemical Reviews*, 44(1):233–244, 1949. doi: 10.1021/cr60137a013.

[18] A. Riaz and H. A. Tchelepi. Numerical simulation of immiscible two-phase flow in porous media. *Phys. Fluids*, 18(1):14104, 2006.

[19] G. Soave. Equilibrium constants from a modified redlich-kwong equation of state. *Chemical Engineering Science*, 27(6):1197–1203, 1972. doi: 10.1016/0009-2509(72)80096-4.

[20] D. V. Voskov and H. A. Tchelepi. Comparison of nonlinear formulations for two-phase multi-component eos based simulation. *Journal of Petroleum Science and Engineering*, 82-83:101–111, 2012.

[21] D.V. Voskov, H. Henley, and A. Lucia. Fully compositional multi-scale reservoir simulation of various co2 sequestration mechanisms. *Computers and Chemical Engineering*, 96:183–195, 2017. doi: 10.1016/j.compchemeng.2016.09.021.

[22] R. Zaydullin, D.V. Voskov, S.C. James, and A. Lucia. Fully compositional and thermal reservoir simulation. *Computers and Chemical Engineering*, 63:51 – 65, 2014.

[23] Y. Zhou, H.A. Tchelepi, and B.T. Mallison. Automatic differentiation framework for compositional simulation on unstructured grids with multi-point discretization schemes. *SPE Reservoir Simulation Symposium*, 2 2011.

[24] Y. Zhou, H.A. Tchelepi, and B.T. Mallison. Automatic differentiation framework for compositional simulation on unstructured grids with multi-point discretization schemes. In *Society of Petroleum Engineers - SPE Reservoir Simulation Symposium 2011*, volume 1, pages 607–624, 2011.